Preprint
UCRL-JC-153466

Electric field enhancement by nodular defects in multilayer coatings irradiated at normal and 45° incidence

C. J. Stolz, F. Y. Génin and T. V. Pistor

Boulder Damage Symposium XXXV
Annual Symposium on Optical Materials for High Power Lasers
Boulder, Colorado September 22-24, 2003

U.S. Department of Energy

Lawrence
Livermore
National
Laboratory

September 18, 2003

Electric-field enhancement by nodular defects in multilayer coatings irradiated at normal and 45° incidence

Christopher J. Stolz[a], Francois Y. Génin[a], Thomas V. Pistor[b]
[a]University of California, Lawrence Livermore National Laboratory,
7000 East Avenue L-491, Livermore, CA 94550
[b]Panoramic Technology Inc., 154 Panoramic Way, Berkeley, CA 94704

ABSTRACT

The standing-wave electric-field profile within multilayer coatings is significantly perturbated by a nodular defect. The intensity, which is proportional to the electric field squared, is increased in the high index material by ≥3× at normal incidence and ≥12× at 45 degrees incidence angle. Therefore it is not surprising that nodular defects are initiation sites of laser-induced damage. In this study, the impact of reflectance-band centering and incident angle are explored for a 1 μm diameter nodular defect seed overcoated with a 24 layer high-reflector constructed of quarter-wave thick alternating layers of hafnia and silica. The modeling was performed using a three-dimensional finite-element analysis code.

Keywords: Standing-wave electric field, nodular defect, multilayer coating, laser damage, finite-element analysis

1. INTRODUCTION

Calculations by DeFord[1] demonstrated a standing-wave electric-field (SWEF) enhancement at normal incidence due to the nodular defect. Sawicki[2] later calculated temperature rises and thermomechanical stresses due to this SWEF enhancement to generate a model of nodular ejection. In these calculations, the SWEF code was limited to calculations of rotationally-symmetric two-dimensional cases. Such codes limited the calculation to normal incidence cases and neglected polarization effects. Improvements in computational speed, memory and in finite-element codes have recently allowed three-dimensional calculations of cases at oblique incidence with polarization effects.

Experimental studies have determined that the laser-induced damage threshold (LIDT) at nodular defects decreases as the seed diameter increases.[3-4] A fracture-based model suggests a critical defect seed diameter exceeding 0.7 μm and a nodule diameter exceeding 4 μm.[5-6] This work assumes that the high-reflectance angular bandwidth of the coating is narrower than the range of incident angles due to the geometry of the nodular defect. Damage studies of large-aperture (40 cm × 40 cm) optics[7] have fluence-limiting damage sites with deep nodular-ejection pits. Therefore, in order to model a relevant geometry, the nodular defect selected for this modeling work is a deep 1-μm diameter seed with a nodular diameter of 5.6 μm.

2. GEOMETRY

A theoretical nodular defect, as is illustrated in figure 1, was used for this study. The nodular-seed diameter selected is 1 μm. The particle that created the nodule is on the substrate surface. A quarter-wave reflector design [air:L(LH)^{12}:glass] consisting of 24 alternating layers of hafnia and silica covers the seed. The reference wavelength is 1053 nm and the refractive indices of the layers are $n_H = 1.971$ and $n_L = 1.44977$. The physical thicknesses of each hafnia and silica layer are 133.56 nm and 181.58 nm respectively. The total film thickness is 3.96 μm. The stack is overcoated with a half-wave silica layer to improve laser

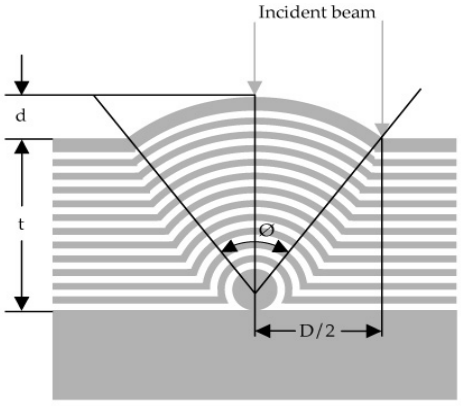

Figure 1. Geometry of a theoretical nodular defect

resistance.[8-9] Assuming uniform deposition over the spherical seed, a parabola defines the boundary between the perfect stack and the nodule. The nodular-defect diameter (D), seed diameter (d), and film thickness (t) obey the following relation[10]:

$$D = \sqrt{8dt} \qquad \text{Eqn. 1}$$

In the case modeled, the nodular defect diameter is 5.6 μm. Given the hemispherical shape of the defect, the nodular defect has an angular range defined by equation 2.

$$\phi = 2\cos^{-1}\left[\frac{2t-d}{2t+d}\right] \qquad \text{Eqn. 2}$$

For this geometry, the incident-angular range of the nodule is 78 degrees. At normal incidence to the defect-free region of the coating, the incidence-angle range (θ) of the defect is

$$0 \le \theta \le \frac{\phi}{2} \qquad \text{Eqn. 3}$$

For this geometry, the incidence-angular range is 0 to 39 degrees.

If the laser beam hits the defect-free region of the coating at an oblique incidence angle (θ_i), the incidence angle range of a nodular defect (θ) is now given by:

$$\theta_i - \frac{\phi}{2} \le \theta \le \theta_i + \frac{\phi}{2} \qquad \text{Eqn. 4}$$

which is limited to angles between 0 and 90 degrees. At a 45 degree oblique incidence angle, the incidence angular range of the defect for this geometry is 6 to 84 degrees.

For both normal and oblique incidence cases, polarization effects become significant because the nodular defect is exposed to a range of incidence angles and opposite polarizations at orthogonal cross sections. As illustrated in figure 2, a nodule exposed to a linearly polarized laser beam is actually exposed to both "S" and "P" polarization (TE and TM) for both normal and oblique incidence.

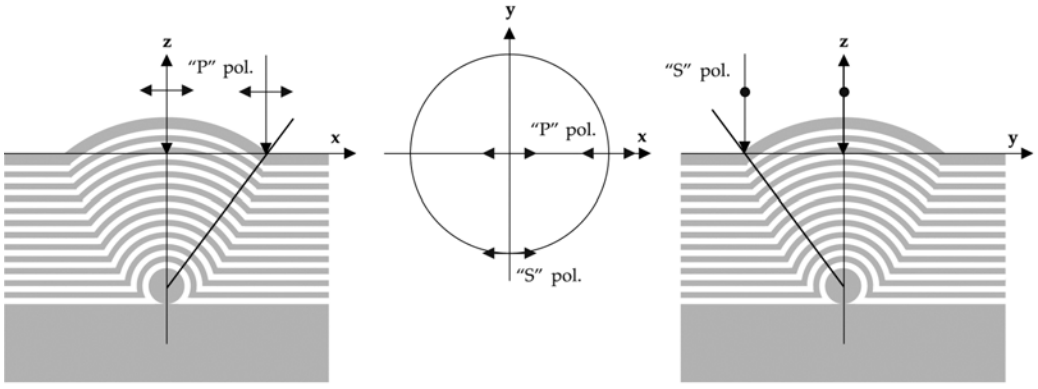

Figure 2a. Normal incidence irradiation of a nodular defect has different polarization orientations for orthogonal cross sections.

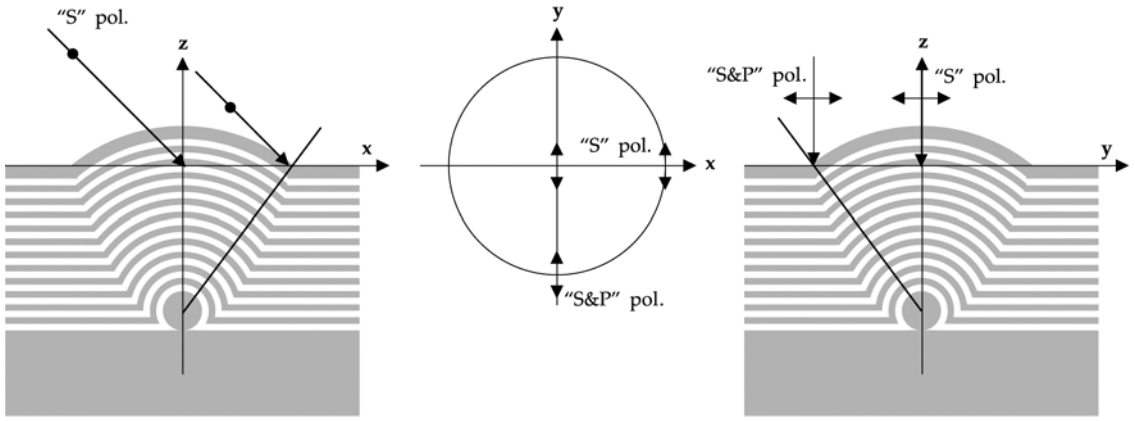

Figure 2b. Oblique incidence irradiation of defects have compound angles that leads to polarization mixing.

Since optical coatings have a finite spectral angular bandwidth and nodular defects have a wide angular range, the impact of spectral centering can be significant. During manufacturing of laser mirrors, spectral centering is achieved by changing the thickness of the individual layers as illustrated in figure 3. From a modeling perspective, it is much easier to maintain a constant geometry while varying the wavelength to achieve the same purpose.

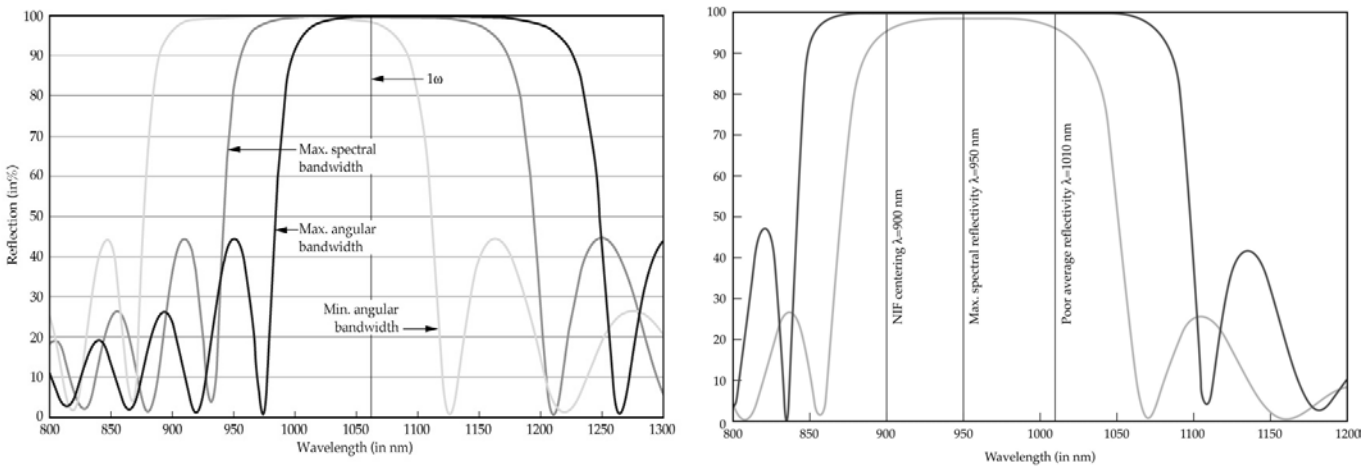

Figure 3. Spectral centering impacts angular bandwidth of the coating for a monochromatic source (left image). This effect can be modeled by maintaining optical thickness and varying irradiating wavelength (right image).

For the modeled coating, increasing the irradiation wavelength increases the angular range of the high-reflectance region of the coating as illustrated in figure 4. From this information, wavelengths for minimum and maximum angular bandwidth can be calculated.

At oblique incidence the phase thickness for a thin film is[11]

$$\frac{\delta = 2\pi nd\cos\theta_i}{\lambda}. \qquad \text{Eqn. 5}$$

Therefore, the wavelength of the center of the reflectance band decreases with increasing incident angle. One minor disadvantage of this approach of keeping the model constant, irradiating at oblique incidence, and varying the wavelength, is the coatings are no longer exactly a quarter-wave thick. However, for the 45 degree incidence case, the thickness differences are relatively small. The hafnium layers are 1.3% thinner than a half wave and the silica layers are 5.1% thicker than a half wave.

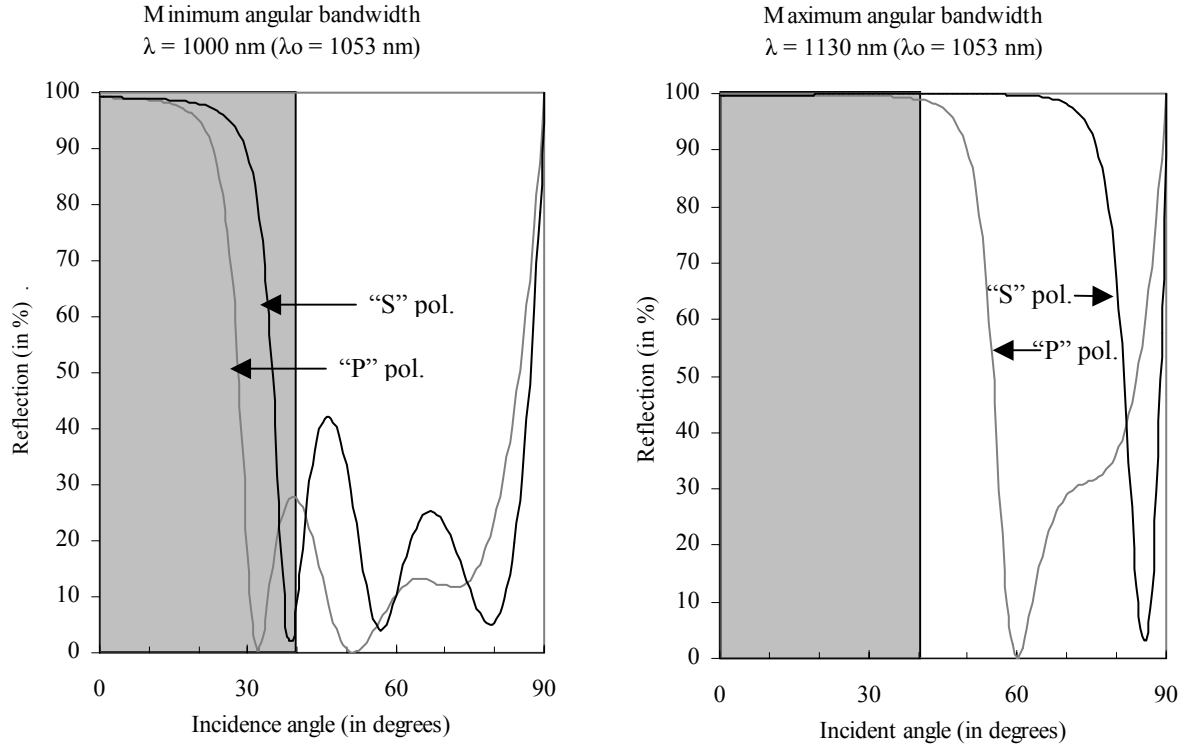

Figure 4. Increasing the centering wavelength increase the angular high reflection bandwidth

3. FINITE ELEMENT ANALYSIS CODE

The TEMPEST[12-13] program is an implementation of the Finite-Difference Time-Domain algorithm proposed by Yee[14] as a technique for solving the Maxwell equations. The TEMPEST algorithm for this study simulates the scattering of an electromagnetic plane wave by a defective multilayer mirror topography. The materials in the multilayer coating and defect seed are specified by their complex optical indices of refraction. The simulation domain is rectangular, three-dimensional, and gridded with a uniform rectangular grid. Periodic boundary conditions are applied in the x- and y-directions while Berenger's perfectly matched layer (PML) absorbing boundary condition[15] is applied in the z- direction.

The rectangular simulation domain was gridded using 300 cells in the x and y directions. The cell size in the z- direction was chosen to be one-seventh the bi-layer thickness and resulted in 122 cells in the z- direction. Each bi-layer consists of 3 cells for the hafnia layer which underestimates the physical thickness of a quarter wave layer at 1053 nm by 0.8%. The silica layers with a lower refractive index, and hence greater physical thickness at 4 cells, are overestimated by 1.1%. The gridding led to approximately 500 Mbyte simulations with approximately two-hour run times on a 1.6 GHz Personal Computer.

Because the TEMPEST algorithm employs periodic boundary conditions in the x and y (horizontal) direction, it was necessary to stop the algorithm after a set of cycles to prevent scattering interactions between neighboring periods of the periodic topography. This is called "temporal isolation". It was determined that 18 cycles were sufficient to provide the necessary temporal isolation yet still allow a local convergence within the defect topography.

Additionally, the strict periodic boundary conditions used in TEMPEST restrict the incident plane wave angle of incidence to a discrete set of values given by:

$$\frac{Sin\theta_i \bullet m\lambda}{L_x} \qquad \text{Eqn. 6}$$

where m is an integer and L_x is the length of the simulation domain in the x- direction. To achieve a 45 degree incidence for the three wavelengths used at 45 degrees, the length of the simulation domain had to be adjusted as shown in table 1.

Table 1: Impact of wavelength and incidence angle on the length simulation domain.

Case	Wavelength (in nm)	Angle of incidence (in degrees)	Polarization	Lx, Ly (in μm)
1	1000	0	-	15.0000
2	1053	0	-	15.0000
3	1130	0	-	15.0000
4	900	45	TE	15.2735
5	900	45	TM	15.2735
6	932.5	45	TE	14.5063
7	932.5	45	TM	14.5063
8	965	45	TE	15.0119
9	965	45	TM	15.0119

4. RESULTS

4.1 Normal incidences (0 degree)

Three wavelengths were selected for normal incidence modeling as illustrated in figure 5. The coating is centered at $\lambda_0 = 1053$ nm. At a wavelength of $\lambda = 1000$ nm, a very high reflectivity occurs over the entire angular range of the nodule. At $\lambda = 1130$ nm, the angular range of high reflectance is reduced resulting in significantly greater transmission at the outer boundary of the nodule.

The SWEF profiles of a nodular defect irradiated at normal incidence at three different wavelengths are shown in figure 6. The peak intensity $\langle |E|^2 \rangle$ of the SWEF enhancement ranges from 3.1× to 9.2× depending on the illumination wavelength. The SWEF peaks are along the central axis and are located near the top of the nodule for the two highest average reflecting cases. The nodule with the smallest angular bandwidth has a SWEF peak at the bottom of the nodule within the defect seed.

The SWEF enhancement is high at the edge of the nodule where the transmission is highest. For real defects (non ideal), the boundary between the nodule and film for defects in coatings is typically quite distorted. Therefore, it is likely that this boundary will be susceptible to damage. A high SWEF within the nodule seed is also problematic. Evidence of molten seeds[16] suggests poor stoichiometry that would result in enhanced thermal and therefore, enhanced stress gradients

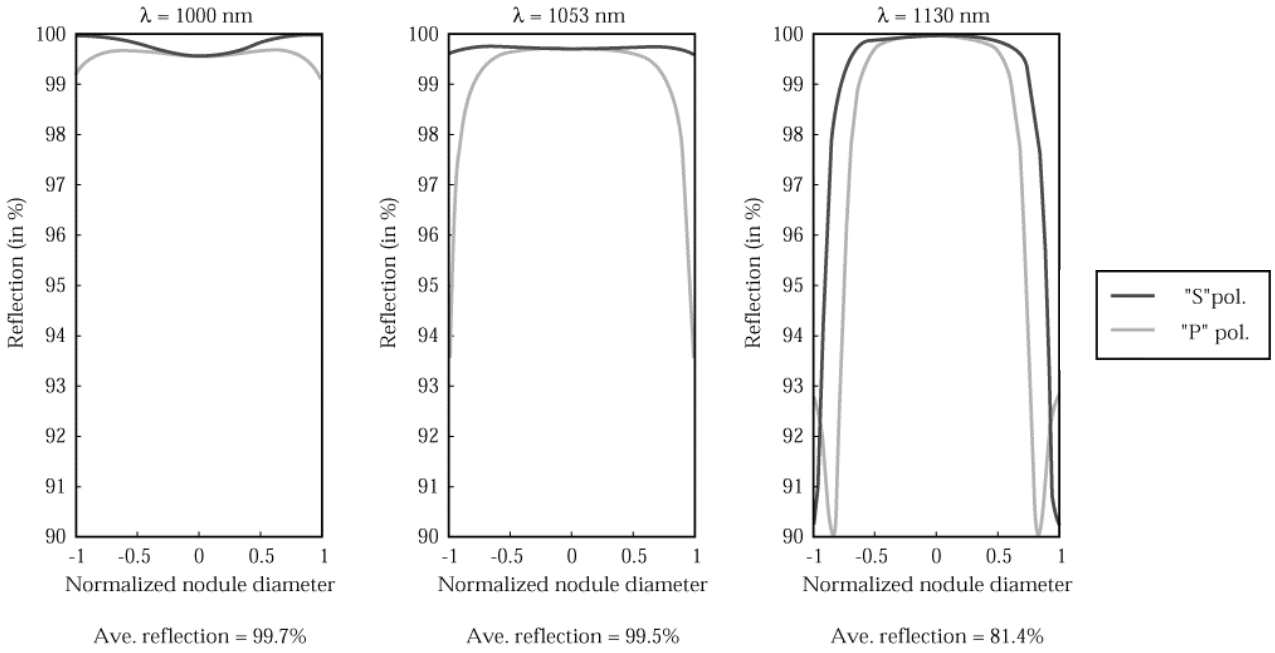

Figure 5. the average reflectance of a nodular defect irradiated at normal incidence is maximized by reducing the incident wavelength.

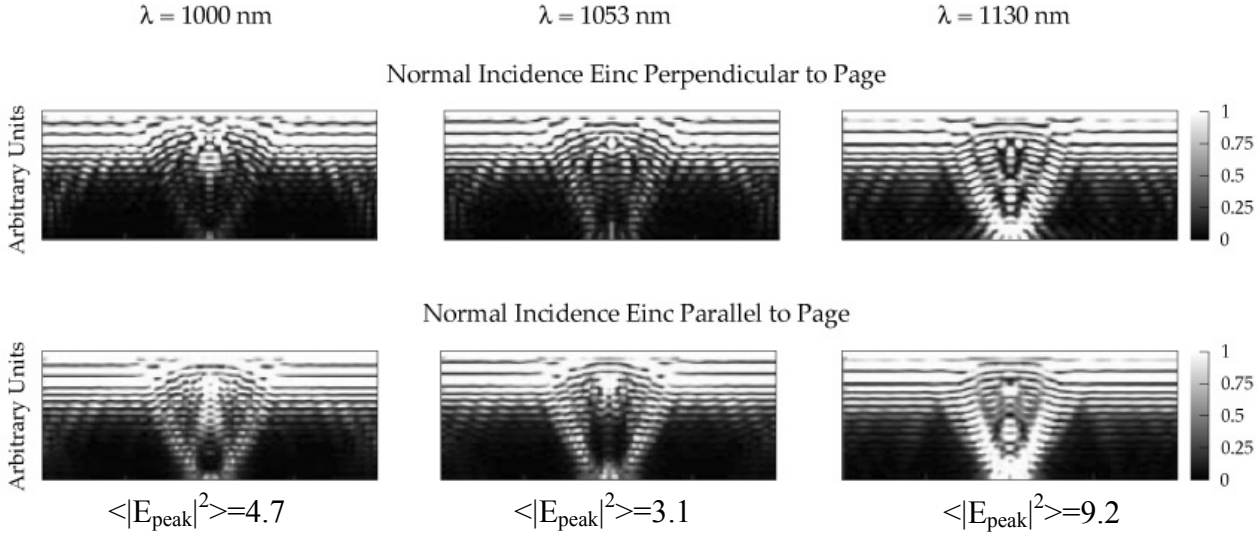

Figure 6. SWEF profiles of a nodular defect illuminated at normal incidence illustrates intensity enhancements $<|E|^2>$ ranging from 3.1× to 9.2×.

4.2 Oblique incidence (45 degree)

Three wavelengths were also selected at the left edge, center, and right edge of the reflector stack at 900, 950, and 1010 nm respectively. The average reflectivity over the angular range of the nodule ranges from 72.5% to 88.8% with reflection zones less than 10% present at each wavelength as illustrated in figure 7. At normal incidence the reflectivity does not drop below 90%. Therefore, a higher SWEF profile is expected over the normal incidence cases, since the transmission of light at the nodule is higher at oblique incidence.

The peak intensity of the SWEF $<|E|^2>$ ranges from 11.5× to 23.4× depending on the incident wavelength and polarization as illustrated in figure 8. The maximum SWEF falls along a line nominally parallel to the incident angle and

extends to the interface between the nodule and thin film. The SWEF is significantly higher than the normal incidence case. As mentioned in the normal irradiance section, the boundary between the nodule and multilayer can be quite distorted so a high SWEF is undesirable at this interface from a laser resistance perspective. Also a high SWEF within the seed is a likely source of high internal stresses as mentioned previously.

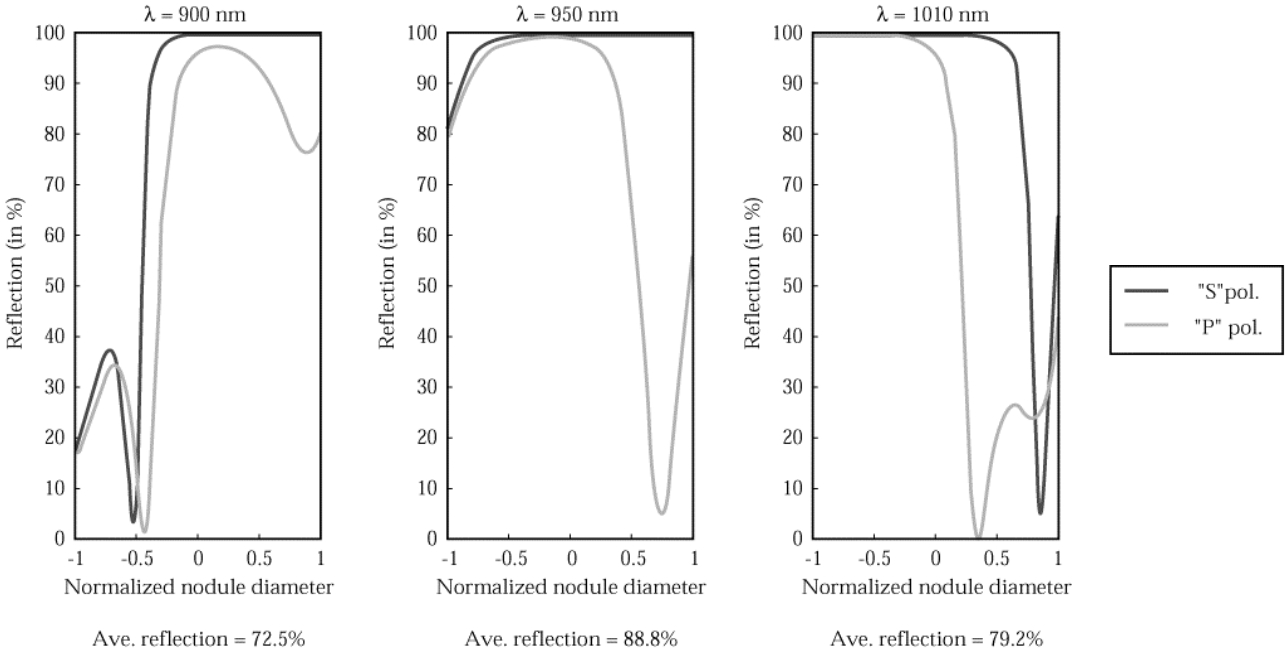

Figure 7. Wavelength centering maximizes the average reflectance of a nodular defect irradiated at oblique incidence.

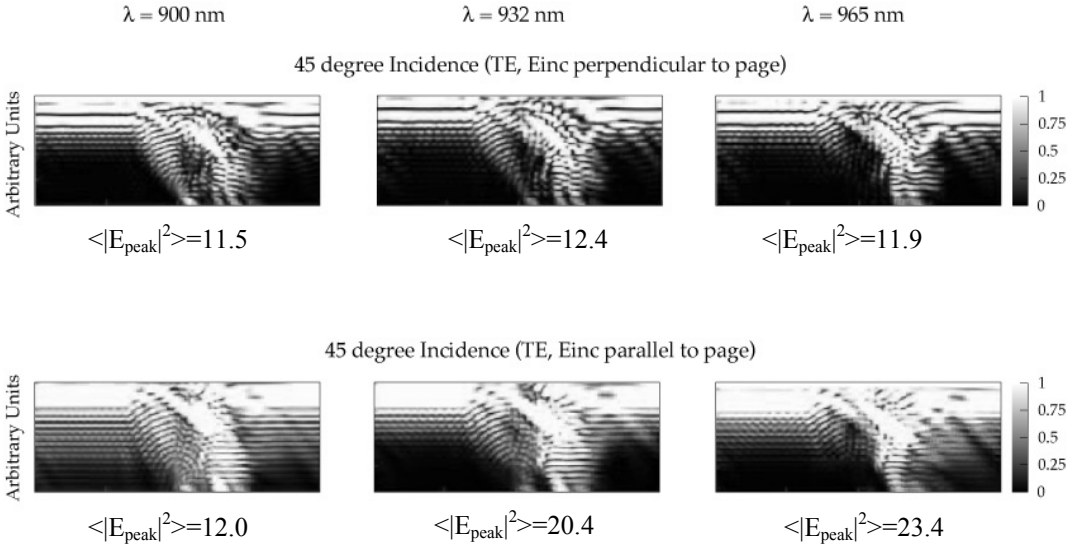

Figure 8. SWEF profiles of a nodular defect illuminated at oblique incidence illustrates intensity $<|E|^2>$ enhancements ranging from 11.5× to 23.4×

5. CONCLUSIONS

Although the SWEF profile is quite low at the bottom of a defect-free coating, significant SWEF enhancements are observed in deeply imbedded coating nodules. Irradiation at oblique incidence angles only exaggerates these effects as illustrated by the ≥3× versus ≥11× intensity enhancement for normal versus oblique incidence respectively. Coating centering has an impact on the SWEF profile. The SWEF profile is most significantly reduced at oblique incidence by reducing the irradiation wavelength (or increasing the centering wavelength). This phenomenon can be explained by the angular bandwidth of the reflection band of the coating. Polarization also becomes significant, particularly at oblique incidence because of the decreased angular range of the reflectance band. Electric-field enhancement clearly explains why laser damage in optical coatings is so easily triggered by nodular inclusions.

AKNOWLEDGEMENTS

The authors would like to acknowledge the support of Andrea Flammini in preparing this manuscript and Mark McDaniel for assistance with the graphics. This work was performed under the auspices of the U. S. Department of Energy by the University of California, Lawrence Livermore National Laboratory under Contract No. W-7405-Eng-48.

REFERENCES

1. J. F. DeFord and M. R. Kozlowski, "Modeling of electric-field enhancement at nodular defects in dielectric mirror coatings", in *Laser-Induced Damage in Optical Materials: 1992*, H. E. Bennett, L. L. Chase, A. H. Guenther, B. E. Newnam, and M. J. Soileau, eds., Proc. SPIE. **1848**, 455-470 (1993).
2. R. H. Sawicki, C. C. Shang, and T. L. Swatloski, "Failure characterization of nodular defects in multi-layer dielectric coatings", in *Laser-Induced Damage in Optical Materials: 1994*, H. E. Bennett, A. H. Guenther, M. R. Kozlowski, B. E. Newnam, and M. J. Soileau, eds., Proc. SPIE. **2428**, 333-342 (1995).
3. R. J. Tench, R. Chow, M. R. Kozlowski, "Characterization of defect geometries in multilayer optical coatings", J. Vac. Sci. Technol. A **12**, 2808-2813 (1994).
4. M. R. Kozlowski, R. J. Tench, R. Chow, and L. Sheehan, "Influence of defect shape on laser-induced damage in multiplayer coatings", in *Optical Interference Coatings*, F. Abelès, ed., Proc. SPIE. Eng. **2253**, 743-750 (1994).
5. J. Dijon, M. Poulingue, J. Hue, "Thermomechanical model of mirror laser damage at 1.06 mm. Part 1: nodule ejection", in *Laser-Induced Damage in Optical Materials: 1998*, G. J. Exarhos, A. H. Guenther, M. R. Kozlowski, K. L. Lewis, and M. J. Soileau, eds., Proc. SPIE Eng. **3578**, 387-396 (1999).
6. M. Poulingue, M. Ignat, and J. Dijon, "The effects of particle pollution on the mechanical behaviour of multilayer systems", Thin Solid Films **348**, 215-221 (1999).
7. J. Taniguchi, N. E. LeBarron, J. Howe, D. J. Smith, C. J. Stolz, C. L. Weinzapfel, and J. F. Kimmons, "Functional damage thresholds of hafnia/silica coating designs for the NIF laser", in *Laser-Induced Damage in Optical Materials: 1999*, G. J. Exarhos, A. H. Guenther, M. R. Kozlowski, K. L. Lewis, and M. J. Soileau, eds., Proc. SPIE **4347**, 109-117 (2000).
8. C. C. Walton, F. Y. Génin, M. R. Kozlowski, G. E. Loomis, and E. Pierce "Effect of silica overlayers on laser damage of HfO_2-SiO_2 56˚ incidence high reflectors," in *Laser-Induced Damage in Optical Materials: 1995*, H. E. Bennett, A. H. Guenther, M. R. Kozlowski, B. E. Newnam, and M. J. Soileau, eds., Proc. SPIE **2714**, 550-558 (1996).
9. C. J. Stolz, F. Y. Génin, T. A. Reitter, N. Molau, R. P. Bevis, M. K. Von Gunten, D. J. Smith, and J. F. Anzellotti, "Effects of SiO_2 overcoat thickness on laser damage morphology of HfO_2/SiO_2 Brewster's angle polarizers at 1064 nm", in *Laser-Induced Damage in Optical Materials: 1996*, H. E. Bennett, A. H. Guenther, M. R. Kozlowski, B. E. Newnam, and M. J. Soileau, eds., Proc. SPIE **2966**, 265-272 (1996).
10. T. Spalvins and W. A. Brainard, "Nodular growth in thick-sputtered metallic coatings", J. Vac. Sci. Technology **11**, 1186- 1192 (1974).
11. A. Macleod, *Thin-film optical filters*, 3rd ed. (Institute of Physics Publishing, Bristol, UK, 2001), Chap. 8.
12. A. Wong, "Rigorous three-dimensional time-domain finite-difference electromagnetic simulation", Ph. D. Dissertation, University of California at Berkeley (1994).

13. T. Pistor, “Electromagnetic simulation and modeling with applications in lithography”**,** Ph. D. Dissertation, University of California at Berkeley (2001).
14. K. S. Yee, “Numerical solution of initial boundary value problems involving Maxwell’s equations in isotropic media”, IEE Trans. Ant. Prop. **14**, 302-307 (1966).
15. J. Berenger, “A perfectly matched layer for the absorption of electromagnetic waves”, J. of Comp. Phys. **114**, 185-200 (1994).
16. C. J. Stolz, R. J. Tench, M. R. Kozlowski, and A. Fornier “A comparison of nodular defect seed geometeries from different deposition techniques” in *Laser-Induced Damage to Optical Materials: 1995*, H. E. Bennett, A. H. Guenther, M. R. Kozlowski, B. E. Newnam, and M. J. Soileau, eds., Proc. SPIE **2714**, 374-382, (1996).